Hindawi Publishing Corporation
Shock and Vibration
Volume 2016, Article ID 6196542, 14 pages
http://dx.doi.org/10.1155/2016/6196542

Research Article

Energy Conservation Analysis and Control of Hybrid Active Semiactive Suspension with Three Regulating Damping Levels

Long Chen,[1] Dehua Shi,[1] Ruochen Wang,[1] and Huawei Zhou[2]

[1]*School of Automotive and Traffic Engineering, Jiangsu University, Zhenjiang 212013, China*
[2]*School of Electrical and Information, Jiangsu University, Zhenjiang 212013, China*

Correspondence should be addressed to Long Chen; chenlong@ujs.edu.cn

Received 3 June 2015; Revised 13 September 2015; Accepted 4 October 2015

Academic Editor: Edoardo Sabbioni

Active suspension has not been popularized for high energy consumption. To address this issue, this paper introduces the concept of a new kind of suspension. The linear motor is considered to be integrated into an adjustable shock absorber to form the hybrid active semiactive suspension (HASAS). To realize the superiority of HASAS, its energy consumption and regeneration mechanisms are revealed. And the system controller which is composed of linear quadratic regulator (LQR) controller, mode decision and switch controller, and the sliding mode control based thrust controller is developed. LQR controller is designed to maintain the suspension control objectives, while mode decision and switch controller decides the optimal damping level to tune motor thrust. The thrust controller ensures motor thrust tracking. An adjustable shock absorber with three regulating levels to be used in HASAS is trial produced and tested to obtain its working characteristics. Finally, simulation analysis is made with the experimental three damping characteristics. The impacts of adjustable damping on the motor force and energy consumption are investigated. Simulation results demonstrate the advantages of HASAS in energy conservation with various suspension control objectives. Even self-powered active control and energy regenerated to the power source can be realized.

1. Introduction

Active suspension can coordinate the trade-off between ride comfort and handling performance according to the control targets and improve suspension dynamic performance significantly. Compared with hydraulic and pneumatic actuators, electromagnetic actuators have smaller response time and wider effective bandwidth. Therefore, electromagnetic actuators attract more attention in the recent years [1–3]. However, shortcomings of active suspension in high energy consumption, high cost, and poor reliability in emergencies prevent it from being widely used and commercialized [4]. To address this urgent issue, on one hand, energy-harvesting techniques are combined with active suspension to reduce the energy consumption; on the other hand, the concept of hybrid active-passive suspension (HAPS) is proposed [5–7].

As for energy harvesting techniques, both new energy regenerative structures and control theories have been disseminated in references. Suda et al. adopted two linear DC motors to realize active control and energy regeneration. One of the DC motors acts as an energy regenerative damper to harvest vibration energy, while another one was used as an actuator to realize active control with the reclaimed energy [8]. In 2003, Nakanoa et al. further presented a method to evaluate the balance between suspension regenerated and consumed energy. The possibility to suppress the suspension vibration with regenerated energy by using a single electric actuator was investigated. And the practical system was also proposed [9]. Zhang et al. designed active and energy regenerative controllers to maintain ride comfort and energy regeneration, respectively. The results indicated that although ride comfort was not as good as that under active control, energy regeneration into the battery was obtained [10]. Zuo et al. proposed different kinds of electromagnetic dampers; most of them acted as passive dampers to recuperate vibration energy. Therefore, these energy-harvesting shock absorbers are weak in the improvement of the suspension dynamic performance [11–13].

HAPS is a combination of active actuator and passive damper (hydraulic or electromagnetic). Such new mechanism justifies less energy consumption and lower cost but the same performance compared with the active suspension. Meanwhile, the passive unit still provides passive damping force in case of emergencies. In 2006, Hitachi exhibited an electromagnetic suspension that consists of a hydraulic damper and a tubular linear motor which acts as an actuator. Therefore, it has advantages in response time and ride comfort [14]. Ebrahimi et al. designed two configurations for the hybrid damper mechanism. One of the configurations is designed based on the eddy current losses phenomenon, while another one is integrated with a monotube shock absorber, and the oil damping provides the essential passive damping. The controllable force of both of these two configurations is provided by electromagnetic unit [15, 16]. Martins et al. proved superiority of such suspension in reducing energy consumption and retaining the active suspension performance based on a two-DOF vehicle suspension model [17]. And the impact of passive damping value on suspension performance and power consumption was analyzed through simulation [18].

However, the damping of passive unit is certain. Once the required force of HAPS is decided, the actuator active force is also determined. Therefore, although HAPS allows the motor with lower rated capacity and maintains fail safety, the actuator operating points are uniquely decided by the passive damping with certain control target (certain suspension force), and reduction in energy consumption is limited. What is more, ride comfort and road holding performance are hard to be balanced. Better ride comfort often requires a relative low damping. If the passive damping is high, the actuator needs to operate in motor mode to lower the damping. And if the passive damping is too low, it is also hard to ensure fail safety and HAPS fails to reduce energy consumption distinctly. Due to its various damping values, it is viable for adjustable shock absorber to be used in active suspension to regulate the actuator force for the purpose of lower energy consumption and higher energy regeneration.

Although adjustable shock absorber varies in principles and structures, they can be classified into two main different categories. One of the categories is that the viscosity of the medium can be adjusted, while the other kind is that with adjustable orifices to change the oil throttling area [19, 20]. There is no doubt that a continuous adjustable shock absorber can tune the actuator force in a wide range. However, it will increase the demand for the system on controller development to harmonize shock absorber and actuator. Limited several basing damping levels may be a better choice. For that the shock absorber with adjustable orifices has superiority in simple structure, low cost, and safety, the adjustable shock absorber with three damping states is introduced in HASAS [21]. Besides, considering that the linear electromagnetic actuator has now been priority selection in the vehicle suspension system for fast response, compact structure, and linear motion without motion transformation mechanism, this paper integrates linear motor into the adjustable shock absorber paralleled with a coil spring and proposes the concept of HASAS with three regulating damping levels. Such suspension system is rarely reported in the existing literatures. A mode decision and switch controller is further developed to decide optimal damping level of adjustable shock absorber. Considering that force tracking of the linear motor has a great influence on the suspension vibration isolation and energy regeneration performance while in many literatures the actuator dynamics and influence of actuator servo-loop on the system control performance are often ignored, the sliding mode control based thrust controller is designed to maintain force tracking. The LQR controller, as the outermost loop, is employed to weigh ride comfort and handling performance.

Specifically, the rest of the paper is divided as follows. In Section 2, the concept and working principle of HASAS is given. Energy consumption principle of linear motor is also presented. Section 3 designs the system controller to decide the damping level and realize motor thrust tracking. The characteristic test of an adjustable shock absorber to be further used is conducted in Section 4 to obtain the three damping characteristics. In Section 5, simulation analysis and systematic comparisons are made to highlight effectiveness of HASAS. At last, Section 6 concludes the paper.

2. Dynamic Model of HASAS

2.1. Overview of the Actuator. The concept of the actuator used in HASAS is depicted in Figure 1. The structure is obtained by integrating the linear motor into an adjustable shock absorber, which is similar to the electromagnetic system in [14], except that the dual-tube oil damper is replaced by an adjustable shock absorber with three regulating levels. Permanent magnet is fixed to the tube of shock absorber while motor windings are linked to the piston rod. In this way, permanent and shock absorber tube are fixed to unsprung mass, while wingding and piston rod are connected to sprung mass. The relative motion between sprung mass and unsprung mass can be damped by linear motor and adjustable shock absorber.

Both the piston rod and the valve of the adjustable shock absorber are provided with orifices in the radial direction. A connecting rod driven by step motor is placed inside the piston rod to regulate the valve's orifice. Therefore, the throttling area of the orifices between the piston rod and the valve is regulated by the step motor. There are three damping states of the adjustable shock absorber. Different damping states (soft, medium, and stiff) correspond to different flowing areas. When adjustable shock absorber operates in stiff state, oil just flows through holes in the piston, which is the same as the traditional oil shock absorber. However, when adjustable shock absorber operates in soft or medium state, another oil flowing path through the orifices of the piston rod and the valve is added besides the channel in the piston to decrease oil damping. And the throttling areas of orifices are different when adjustable shock absorber operates in soft or medium state.

2.2. Model of HASAS. A quarter car model is applied to evaluate the dynamic performance and energy conservation

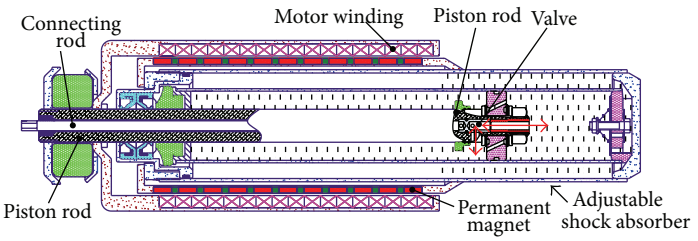

Figure 1: Schematic view of the proposed actuator in HASAS.

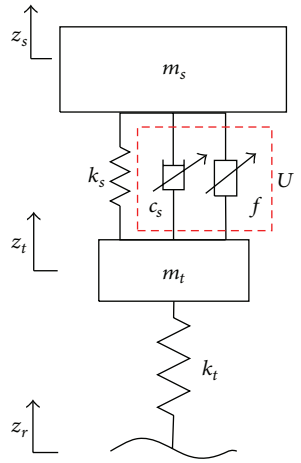

Figure 2: Quarter car model of the proposed active suspension.

of HASAS, as shown in Figure 2. The actuator force can be equivalent to the sum of adjustable damping forceand motor thrust f. Sprung mass and unsprung mass are denoted by m_s and m_t, respectively. The symbols k_s and k_t represent the suspension stiffness and tire stiffness, respectively. Adjustable damping of the shock absorber is marked by c_s. z_s and z_t are vertical displacements of sprung mass and unsprung mass, respectively, while z_r stands for the road displacement.

From the quarter car model of the proposed active suspension, the dynamic equations of the proposed system are depicted as follows:

$$\begin{aligned} m_s\ddot{z}_s &= k_s\left(z_t - z_s\right) + U, \\ m_t\ddot{z}_t &= -k_s\left(z_t - z_s\right) - k_t\left(z_t - z_r\right) - U, \end{aligned} \tag{1}$$

where $U = c_s(\dot{z}_t - \dot{z}_s) + f$.

LQR controller is used to weigh suspension control targets and find relevant optimal force U_{ref} [22]. The criterion function is set as

$$J = \lim_{T\to\infty}\frac{1}{T}\int_0^T \left[q_1\ddot{z}_s^2 + q_2\left(z_s - z_t\right)^2 + q_3\left(z_t - z_r\right)^2\right]dt, \tag{2}$$

where q_1, q_2, and q_3 are weighting coefficients of sprung mass acceleration, suspension, and tire deflection, respectively.

To design the LQR controller, the system dynamic differential equation is transformed into the state-space equation

$$\begin{aligned} \dot{\mathbf{X}} &= \mathbf{AX} + \mathbf{BU} + \mathbf{F}\omega, \\ \mathbf{Y} &= \mathbf{CX} + \mathbf{DU}. \end{aligned} \tag{3}$$

The state vector and output vector are chosen as

$$\begin{aligned} \mathbf{X} &= \left[z_s \;\; z_t \;\; \dot{z}_s \;\; \dot{z}_t \;\; z_r\right]^T, \\ \mathbf{Y} &= \left[\ddot{z}_s \;\; z_s - z_t \;\; z_t - z_r \;\; k_t\left(z_t - z_r\right)\right]^T. \end{aligned} \tag{4}$$

Then the suspension optimal feedback control force is

$$\mathbf{U} = -\mathbf{KX} = \mathbf{R}^{-1}\mathbf{B}^T\mathbf{PX}, \tag{5}$$

where $\mathbf{P}$ can be derived from Riccati equation by

$$\mathbf{A}^T\mathbf{P} + \mathbf{PA} - \mathbf{PBR}^{-1}\mathbf{B}^T\mathbf{P} + \mathbf{Q} = 0, \tag{6}$$

where $\mathbf{Q} = \mathbf{C}^T\mathbf{qC}$, $\mathbf{R} = \mathbf{D}^T\mathbf{qD}$, $\mathbf{N} = \mathbf{C}^T\mathbf{QD}$, $\mathbf{q} = \text{diag}(q_i)$, $(i = 1, 2, 3)$.

The input model of the road surface is simulated by filtered white noise as

$$\dot{z}_r = -2\pi f_0 z_r + 2\pi n_0\sqrt{G_q\left(n_0\right)u}\omega, \tag{7}$$

where ω is the white Gaussian noise of random road inputs. f_0 denotes the lower cut-off frequency, which equals 0.0628 Hz. n_0 is the reference spatial frequency and is recorded as $0.1\,\text{m}^{-1}$. u represents the vehicle velocity and $G_q(n_0)$ is road roughness coefficient.

2.3. Energy Consumption of Linear Motor. The equivalent circuit of motor is modeled as in Figure 3. In the figure, E_a is the induced voltage of linear motor M and L and R are the motor inductance and resistance, respectively. The motor is connected to the power source with the variable voltage E. The circuit equation is

$$E = L\frac{di}{dt} + iR + E_a. \tag{8}$$

Under random road excitation, the induced voltage E_a is given by

$$E_a = K_E v, \tag{9}$$

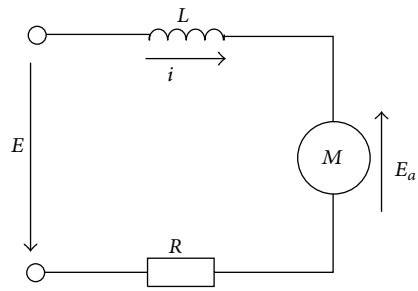

Figure 3: Equivalent circuit model of linear motor.

where K_E is the back electromotive voltage (EMF) constant and v is the motor working velocity. Usually, the motor inductance L can be neglected, and the motor winding current i and thrust f are defined by

$$i = \frac{E - E_a}{R}, \qquad f = K_I i, \tag{10}$$

where K_I is thrust constant.

Assuming that the desired actuator force is U_{ref}, then required thrust f_{ref} of the linear motor is given by

$$f_{\text{ref}} = U_{\text{ref}} - c_s\left(\dot{z}_t - \dot{z}_s\right). \tag{11}$$

Hence, to obtain the desired motor force f_{ref}, required voltage E_{ref} of the power source is obtained by

$$E_{\text{ref}} = \frac{f_{\text{ref}} R}{K_I} + K_E v. \tag{12}$$

And electrical power P_{ele} supplied by the power source is derived as

$$P_{\text{ele}} = \left(\frac{f_{\text{ref}}}{K_I}\right)^2 R + \frac{K_E v}{K_I} f_{\text{ref}}. \tag{13}$$

Besides, the mechanical power of the linear motor is

$$P_{\text{mec}} = f_{\text{ref}} v. \tag{14}$$

When $P_{\text{ele}} < 0$, part of vibration mechanical energy is converted into electrical energy and delivered to the power source. It is defined that linear motor operates in "regeneration mode." While $P_{\text{ele}} > 0$, if $P_{\text{mec}} > 0$, the linear motor works as a motor, and it consumes electrical energy from the power source to acquire the desired thrust. If $P_{\text{mec}} < 0$ and $P_{\text{ele}} > 0$, the energy that is both regenerated by the motor and accepted from the power source is dissipated as heat in the motor resistance. And the linear motor still consumes electrical energy from the power source although it operates as a generator in this case. Therefore, when $P_{\text{ele}} > 0$, the linear motor can be defined by operating in "consumption mode."

If there is no power source to power the motor, the linear motor just operates as a generator to provide the electromagnetic damping force. When the motor windings are directly short circuited, the motor is equivalent to a passive electromagnetic damper depicted by

$$f_{\text{ed}} = -\frac{K_I K_E v}{R}, \tag{15}$$

where f_{ed} is the electromagnetic damping force when the motor windings are directly short circuited; that is, the circuit resistance is R. Furthermore, the following equation is obtained:

$$P_{\text{ele}} = \frac{f_{\text{ref}} R}{K_I^2}\left(f_{\text{ref}} - f_{\text{ed}}\right). \tag{16}$$

Table 1: Comparison between motor thrust and damping force.

Velocity	f_{ref}	Relations between f_{ref} and f_{ed}	P_{ele}	Mode
$v > 0$	$f_{\text{ref}} > 0$	—	$P_{\text{ele}} > 0$	Con
	$f_{\text{ref}} < 0$	$f_{\text{ref}} < f_{\text{ed}}$	$P_{\text{ele}} > 0$	Con
		$f_{\text{ref}} > f_{\text{ed}}$	$P_{\text{ele}} < 0$	Reg
$v < 0$	$f_{\text{ref}} < 0$	—	$P_{\text{ele}} > 0$	Con
	$f_{\text{ref}} > 0$	$f_{\text{ref}} > f_{\text{ed}}$	$P_{\text{ele}} > 0$	Con
		$f_{\text{ref}} < f_{\text{ed}}$	$P_{\text{ele}} < 0$	Reg

From (16), it is convenient to analyze the energy consumption situation P_{ele} and the motor operation mode by comparing f_{ref} and f_{ed}, as shown in Table 1. It can be concluded that $P_{\text{ele}} > 0$ when $|f_{\text{ref}}| > |f_{\text{ed}}|$ or $f_{\text{ref}} \cdot f_{\text{ed}} < 0$. Under this circumstance, the linear motor needs to consume energy from the power source. However, while $|f_{\text{ref}}| < |f_{\text{ed}}|$ and $f_{\text{ref}} \cdot f_{\text{ed}} > 0$, $P_{\text{ele}} < 0$ and the linear motor just operates as a generator could produce enough damping force to isolate the suspension vibration, instead of consuming electrical energy, which is beneficial for reducing the system consumption. Therefore, by regulating the damping of adjustable shock absorber, the linear motor operation thrust is better to be tuned to satisfy $|f_{\text{ref}}| < |f_{\text{ed}}|$ and $f_{\text{ref}} \cdot f_{\text{ed}} > 0$ for the purpose of avoiding high energy consumption and even realize energy recovery.

3. System Controller Scheme

The adjustable shock absorber can be regulated among three damping levels, soft, medium, and stiff, while the linear motor can operate as a motor or generator to realize the transformation between electrical energy and mechanical energy. The block scheme of HASAS system is depicted in Figure 4. In the figure, road displacement z_r, motor actual thrust $f_{m\text{act}}$, and damping value c_{sm} (where $m = a$, b, or c represent soft, medium, and stiff damping, resp.) are the quarter car model control inputs. The controller is composed of the damping mode decision and switch controller, the innermost loop thrust controller, and the outermost loop LQR controller which calculate the ideal control force U_{ref} with the system measurable full state. Based on the damping switch rules of the mode decision and switch controller, the reference linear motor force f_{ref} and the desired damping level c_{sm} are decided. The innermost thrust controller which is based on sliding mode control contributes to the reference

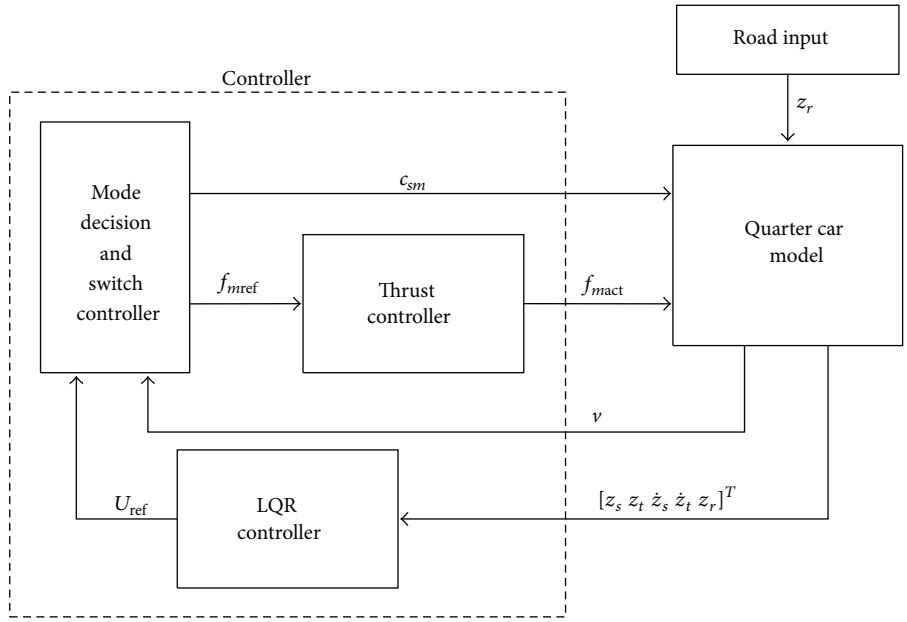

Figure 4: Block scheme of HASAS system.

Table 2: Description of the active suspension operation states.

Operation state of active suspension	Damping level	Mode of linear motor
i	Soft	Reg
ii	Soft	Con
iii	Medium	Reg
iv	Medium	Con
v	Stiff	Reg
vi	Stiff	Con

force tracking (current tracking of linear motor) of the linear motor.

3.1. Mode Decision and Switch. In each damping state of the adjustable shock absorber, the linear motor can operate in "regeneration mode" or "consumption mode" if ignoring the situation $P_{elem} = 0$. Hence, the active suspension with three regulating damping levels totally owes 6 kinds of operation states, as listed in Table 2. At any moment, only one operation state is activated.

3.1.1. Mode Decision Rules. As mentioned previously, the electrical power P_{ele} supplied by the power source is used to evaluate the system energy consumption. Therefore, the instantaneous electrical power P_{ele} under different damping levels is selected as the distinguishing basis for the mode decision and switch controller. And the following basic switch rules are designed:

(1) Preferably, the linear motor should be controlled to operate in "regeneration mode"; that is, the damping coefficient c_{sm} that ensures the linear motor to meet $P_{elem} < 0$ is preferred.

(2) If the motor instantaneous power consumption $P_{elem} > 0$ under all of the three damping levels, it indicates that the motor always operates in "consumption mode" with all the damping levels. In this case, the damping coefficient c_{sm} which meets $\min(\|P_{elem}\|_2)$ is preferred to ensure least energy consumption.

(3) If the motor instantaneous power consumption $P_{elem} < 0$ under all of the three damping levels, the motor always operates in "regeneration mode" to transform part of mechanical energy into electrical energy. Therefore, to recycle more vibration energy, the damping coefficient c_{sm} which meets $\max(\|P_{elem}\|_2)$ is preferred.

Table 3: Relations between N and the motor mode under different damping levels.

Damping level	Operation mode of linear motor							
Soft	Reg	Reg	Reg	Reg	Con	Con	Con	Con
Medium	Reg	Reg	Con	Con	Con	Reg	Reg	Con
Stiff	Reg	Con	Con	Reg	Reg	Reg	Con	Con
N	0	4	6	2	3	1	5	7

3.1.2. Mode Selection Algorithm. According to the optimal control force U_{ref}, the adjustable shock absorber and the linear motor harmonized to produce the required force. The motor operation mode varies with the adjustable shock absorber damping level. And it is detailed in Table 3. Once the damping of the adjustable shock absorber is confirmed, the certain motor thrust is also determined, so is the corresponding energy consumption of the motor. When the adjustable

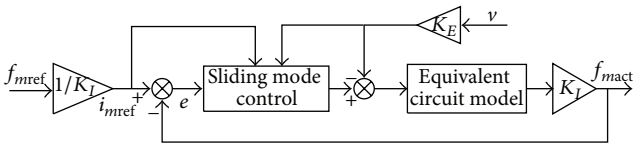

Figure 5: Control scheme of linear motor.

Table 4: Relations between N and the motor optimal power consumption.

N	Motor power consumption	Damping level
0	$\max(\|P_{elem}\|_2)$ $(m = a, b, c)$	Soft or stiff
1	$\max(\|P_{elem}\|_2)$ $(m = b, c)$	Medium or stiff
2	$\max(\|P_{elem}\|_2)$ $(m = a, c)$	Soft or stiff
3	P_c	Stiff
4	$\max(\|P_{elem}\|_2)$ $(m = a, b)$	Soft or medium
5	P_b	Medium
6	P_a	Soft
7	$\min(\|P_{elem}\|_2)$ $(m = a, b, c)$	Soft or stiff

shock absorber operates in soft, medium, and stiff state, the linear motor operation mode is recorded as M_a, M_b, and M_c, respectively. M_a, M_b, and M_c are defined as

$$M_m = \begin{cases} 0, & \text{Regeneration (Reg)}, \\ 1, & \text{Comsumption (Con)}, \end{cases} \quad (m = a, b, c). \tag{17}$$

The state selection function of the proposed active suspension is expressed as

$$N = M_a + 2M_b + 4M_c. \tag{18}$$

In combination with the mode decision rules, the relations between the state selection value N and the motor optimal power consumption are summarized in Table 4. Based on this table, the damping level that ensures best motor operation state can be derived.

3.2. Thrust Controller. Since the damping of the adjustable shock absorber with regulating orifices can be easily realized by controlling the pulse signals of the step motor, the damping characteristics of different damping levels are directly used in the simulation assuming that they can be accurately achieved [23]. And the tracking to the reference thrust is obtained by controlling the motor current through the motor current loop. The thrust controller is designed based on sliding mode control of the current loop and circuit model of linear motor, as shown in Figure 5. Proportional-integral (PI) controller is usually used to tune the controllable power source voltage E to realize the current tracking [24, 25]. However, there is a wide variation of motor circuit parameters when the motor operates in different states. Both changing of system parameters and external disturbance will have a negative influence on the system control. Certain PI control gains cannot ensure good dynamic performance of the force tracking. The nonlinear sliding mode control has an advantage over PI control for its strong robustness with parameter perturbation and external disturbance. And sliding mode control is applied to obtain the required power supply E [26, 27].

When the motor suffers parameters perturbation, the equivalent circuit model is described as

$$E = (L + \Delta L)\frac{di}{dt} + i(R + \Delta R) + K_E(v + \Delta v), \tag{19}$$

where ΔL and ΔR denote the parameters perturbation of motor characteristic parameters and Δv denotes the variation of motor velocity (i.e., suspension relative velocity state) caused by the perturbation. The general perturbation E_r is further defined as

$$E_r = \Delta L\frac{di}{dt} + i\Delta R + K_E\Delta v. \tag{20}$$

Assuming that the current error e between i_{ref} and i is the system state variable and the control input is E, then the error equation of the current loop is given by

$$\dot{e} = -a_r e - b_r u + c_r, \tag{21}$$

where $a_r = R/L$, $b_r = 1/L$, $c_r = (K_E v + Ri_{\text{ref}} + E_r)/L$, and $u = E$ is the control input.

To ensure the sliding modality during the control process and eliminate the system steady-state error, the sliding mode control with integral forms is designed and the sliding line is

$$s = e + c_{im}\int_0^t e(\tau)\,d\tau. \tag{22}$$

c_{im} is the integral coefficient. To ensure that the sliding motion moves towards zero, c_{im} is greater than 0. For the sliding mode control, both the improvement of reaching motion to the sliding modality region and the reduction of system buffeting should be realized. Exponential reaching law of sliding mode control is a good choice to address this issue. And the reaching law is written as

$$\dot{s} = -\varepsilon\,\text{sgn}(s) - \eta s, \tag{23}$$

where ε is the switching gain and η is the exponential coefficient.

According to (21)~(22), u_{eq} is derived as (in this case, E_r is assumed to be 0)

$$u = (Lc_{im} - R)e + Ri_{\text{ref}} + K_E v + \varepsilon\,\text{sgn}(s) + \eta s. \tag{24}$$

To guarantee the existence and accessibility condition of sliding mode control, the chosen Lyapunov function based on Lyapunov stability theory should meet

$$\dot{V} = s\dot{s} < 0. \tag{25}$$

According to (19)~(24), (25) is derived as

$$\begin{aligned} \dot{V} = s\dot{s} &= s\left[-\varepsilon\,\text{sgn}(s) - \eta s + E_r\right] \\ &\le -|s|\left(\varepsilon - |E_r|\right) - \eta s^2. \end{aligned} \tag{26}$$

Therefore, when $\varepsilon > |E_r|$ and $\eta > 0$, the existence and accessibility condition can be realized, and the control system is stable.

Figure 6: Components of the adjustable shock absorber and experimental setup.

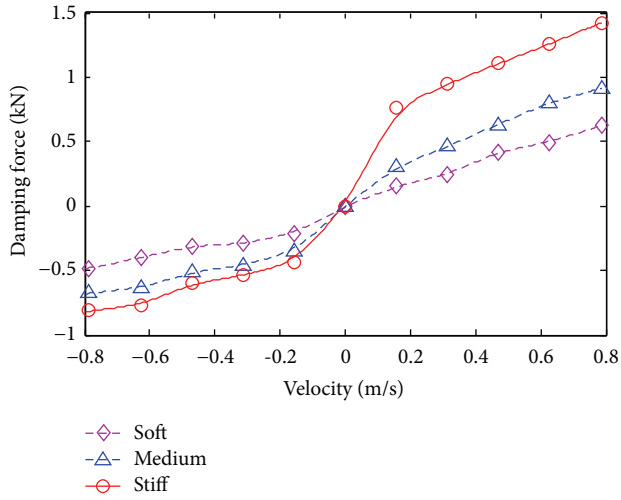

Figure 7: Characteristics of adjustable shock absorber on different damping state.

4. Characteristic Experiments of the Adjustable Shock Absorber

The prototype of adjustable shock absorber to be used is firstly trial produced and tested to obtain its characteristic parameters. The characteristics of the adjustable shock absorber are tested in a hydraulic servo vibration testing machine, as shown in Figure 6. The initial position of the shock absorber is set as equilibrium position. Inputs of the excitation are 50 mm sinusoidal signals with five different frequencies: 0.5, 1.0, 1.5, 2.0, and 2.5 Hz.

Figure 7 describes the force-velocity relationships in different states. Apparently, three different kinds of force-velocity relationships are obtained by regulating the throttling area. For further simulation analysis, the model of adjustable shock absorber is built based on the bench test data of the three force-velocity relationships. By looking up the 2D table and establishing the interpolation algorithm, the damping force of adjustable shock absorber with different velocities is calculated.

Table 5: Parameter of model.

Description	Symbol	Value
Sprung mass	m_s	320 kg
Unsprung mass	m_t	37 kg
Suspension stiffness coefficient	k_s	16 kN/m
Tire stiffness coefficient	k_t	159 kN/m
Thrust constant	K_I	65.7 N/A
Back EMF constant	K_E	53.5 V/(m/s)
Internal resistance	R	4.2 Ω
Pole pitch	τ	71.2 mm
Inductance	L	5.2 mH

Table 6: Weightings for different control targets.

Targets	q_1	q_2	q_3
Handling	0.92	65080	9×10^5
Trade-off	1	4800	3.8×10^4
Ride comfort	4.87	4842	30150

5. Simulation Analysis

In order to validate the effect of the controller and superiority of HASAS in energy conservation, MATLAB/Simulink based simulation model with the designed controller is built. Both random road and bump road are adopted to reveal the responses of the proposed system. Simulation results of the suspension's three evaluation indexes are compared with a passive counterpart whose passive damping coefficient is 1.3 kN·s/m. Simulation parameters are listed in Table 5.

5.1. Random Road Input

5.1.1. Suspension Dynamic Performance. Ride comfort and road holding performance (handling performance) are two critical evaluation indexes of the suspension that are hard to be compromised. Usually, improvement of one criterion leads to the deterioration of the other. As a consequence, three control targets are chosen to judge the HASAS performance: handling, ride comfort, and trade-off, respectively. Handling and ride comfort are intended for the reduction of tire dynamic load and sprung mass acceleration, respectively, while trade-off objective is a compromise between comfort and handling. The principle of trade-off is to improve ride comfort with an acceptable handling performance. The three control targets are realized by adjusting q_1, q_2, and q_3 of LQR controller, as listed in Table 6.

The actual responses of HASAS are compared to the reference responses under LQR control to validate the effectiveness of the designed thrust controller. The random road input is acquired by assuming that the vehicle is driven on C-class road (roughness coefficient is $256 \times 10^{-6}\,\mathrm{m}^3$) at the speed of 20 m/s. The three damping characteristics obtained from bench test are used in the simulation analysis. Figure 8

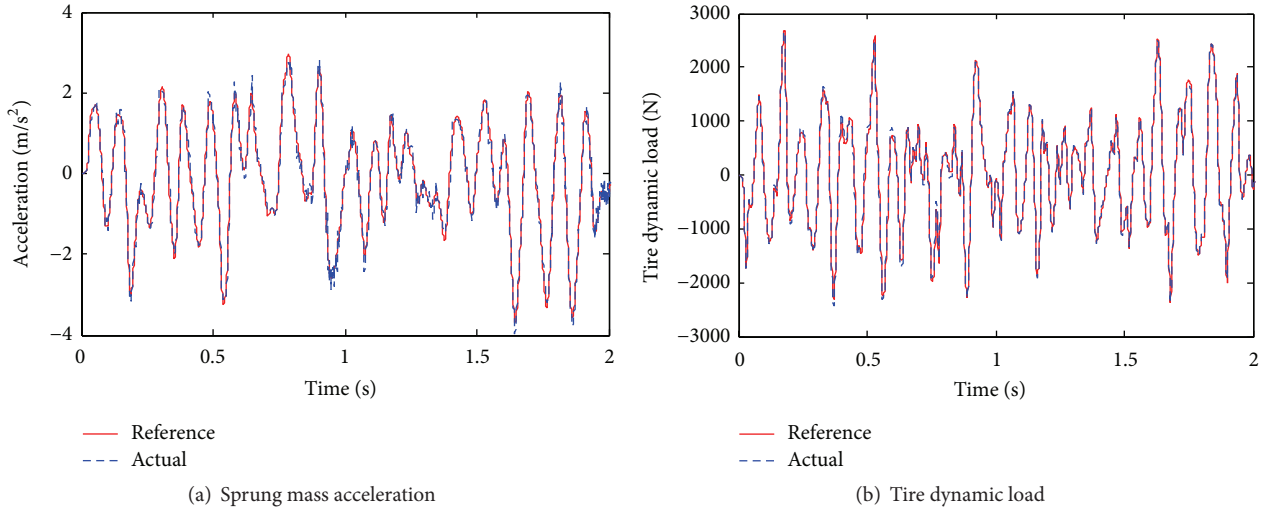

(a) Sprung mass acceleration (b) Tire dynamic load

Figure 8: Actual responses comparing to the reference responses.

Table 7: RMS values of hybrid suspension for the three objectives.

Suspension	Objective	Attribute	a_{rms}/(m/s^2)	SWS_{rms}/m	DTL_{rms}/N
Passive	—		1.660	0.0174	903.7
Hybrid active semiactive	Handling	Reference	2.300	0.0108	690.2
		Actual	2.295	0.0108	699.3
		—	38.25%	−37.93%	−22.62%
	Trade-off	Reference	1.309	0.0140	957.5
		Actual	1.317	0.0140	958.7
		—	−21.14%	−19.54%	6.09%
	Ride comfort	Reference	0.883	0.0178	1338.4
		Actual	0.899	0.0177	1322.7
		—	−45.84%	1.72%	46.36%

gives the sprung mass acceleration and tire dynamic load tracking to the reference responses, while Figure 9 shows time responses of sprung mass acceleration and tire dynamic load between HASAS and passive suspension for the three different control targets. Table 7 describes RMS values of the suspension's three evaluation indexes, including RMS comparisons between actual responses and reference ones, where a_{rms}, SWS_{rms}, and DTL_{rms} represent sprung mass acceleration, suspension deflection, and tire dynamic load, respectively. It can be seen from Figure 8 and Table 7 that the proposed HASAS with designed thrust control can track the reference responses well. As a result, the sliding mode control based thrust controller is effective in HASAS to guarantee motor thrust tracking. Combining Figure 9 and Table 7, it indicates that when handling is emphasized, obvious 37.93% and 22.62% reductions of suspension deflection and tire dynamic load are achieved. When ride comfort is as control target, the visible 45.84% reduction of sprung mass acceleration is obtained at the sacrifice of tire dynamic load, which is increased by 46.36%. For trade-off objective, the attenuation degree of sprung mass acceleration and suspension deflection in HASAS are as much as 21.14% and 19.54%, respectively. Although tire dynamic load is inferior to that of the passive one, the 6.09% deterioration of handling is much smaller than the improvement in ride comfort. It is within acceptable range.

5.1.2. Energy Conservation Performance. To highlight the superiority of HASAS in energy conservation and less dependence on motor rated capacity, the results are analyzed by comparing the linear motor thrust and energy consumption for five cases ulteriorly. In Case A, the active suspension is adopted and suspension force U is provided by the linear motor alone. Cases B, C, and D denote the situation when the adjustable shock absorber is in stiff, medium, and soft state, respectively (also considered as HAPS with different passive damping). And Case E indicates the situation that HASAS is used with mode and switch controller.

In Figure 10, motor force of Cases A and E for trade-off objective is shown. The required peak force in Cases A and E is 1447 N and 618 N, while the required RMS motor force is 425.2 N and 157.6 N, respectively. Furthermore, motor thrust RMS values of the five cases for different control targets are shown in Figure 11. With ride comfort as control target, a large passive damping (stiff state) corresponds to a large motor force, because, for ride comfort, the large damping needs to be lowered by motor. Conversely, large passive damping is

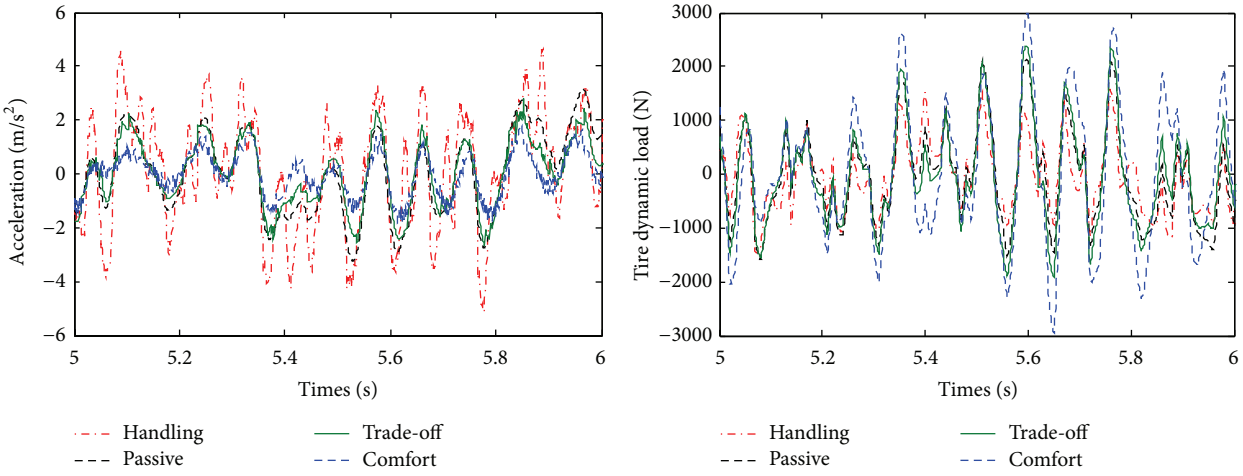

(a) Sprung mass acceleration (b) Tire dynamic load

Figure 9: Actual responses of the proposed suspension comparing to passive suspension.

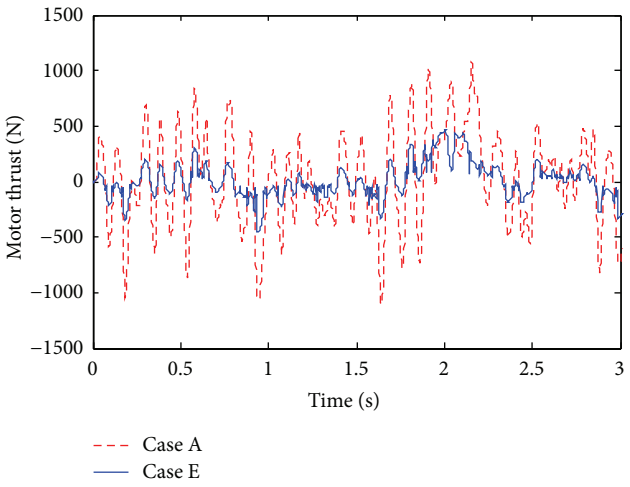

Figure 10: Thrust of the linear motor.

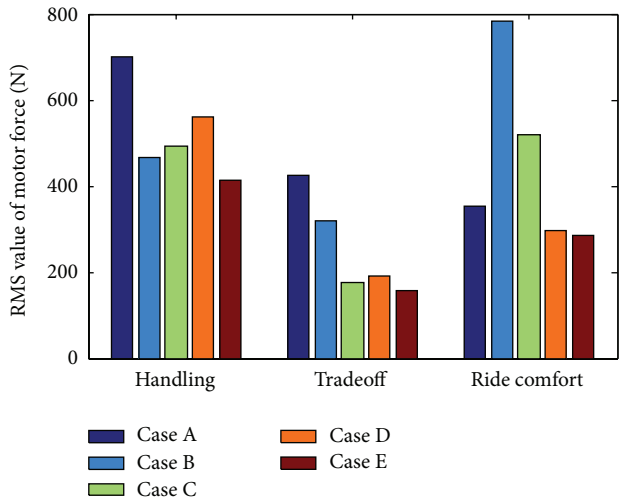

Figure 11: RMS value of motor thrust.

necessary to mitigate the motor force for handling. Compared with the active suspension, the hybrid suspension with large damping is superior in reducing the motor force for handing, while small damping is superior in the motor force reduction for ride comfort objective. It is obvious that a relative high performance of linear motor in terms of rated thrust is required to meet the various control targets with a certain passive damping when HAPS is employed. However, there is no exception that HASAS system requires minimum RMS motor force for all of the three control targets. Therefore, demand for motor rated thrust in HASAS system is reduced apparently for different control targets, which means that lower cost and smaller, lighter motors are allowed.

Suppose that the total electrical energy consumption of the simulation time history (t_{sim}) is W_{tot}, which is obtained by

$$W_{tot} = \int_0^{t_{sim}} P_{ele} dt. \tag{27}$$

Let the simulation time be 30 s; then, energy consumption of linear motor for the three different control targets is shown in Figure 12. It can be seen that active suspension shows less energy consumption for ride comfort (only 74.81 J) and trade-off (1537 J), while a great amount of energy consumption for handling (as much as 1.07×10^4 J). As for Cases B~D, small damping (Case D) causes less energy consumption for ride comfort and trade-off (4982 J for comfort and only 12.84 J for trade-off), while large damping (Case B) leads to much more energy consumption (2.86×10^4 J for ride comfort and 5641 J for trade-off), because linear motor needs to consume more electrical energy to lower the suspension damping. For handling, large damping corresponds to 6154 J energy consumption, while that of small damping is 6972 J. Although energy consumption of HASAS for ride comfort is more than that of active suspension, the advantages of HASAS in energy conservation for trade-off and handling are obvious, especially for trade-off, and the energy consumption is −149.1 J, which means that self-powered active control is

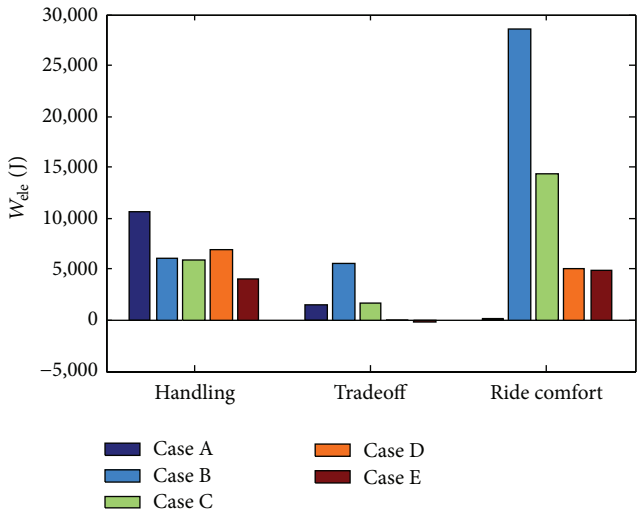

Figure 12: Energy consumption of linear motor.

realized. Therefore, HASAS is a good choice in terms of energy conservation and motor thrust reduction through comprehensive comparisons. To further improve the energy conservation performance, the adjustable range of damping valves can be expanded. It can be inferred that smaller damping value allows better energy conservation performance of HASAS for ride comfort.

To better understand energy consumption of linear motor, comparisons between the electrical power consumption P_{ele} and the motor mechanical power P_{mec} are conducted in Cases A, B, and E for trade-off objective for their typical features, as shown in Figure 13. In Case B, it is apparent that the motor chiefly acts as a motor ($P_{mec} > 0$) to consume electrical energy. However, in Case A, although the motor mainly acts as a generator ($P_{mec} < 0$) in the whole time history, it still consumes a large amount of electrical energy ($P_{ele} > 0$). The reason is that, in Case A, large motor thrust leads to high wingding current; thus both the regenerated energy from suspension vibration and energy acquired from the power source are dissipated by the motor internal resistance as copper losses. In Case E, HASAS realizes energy regeneration ($P_{ele} < 0$) in many regions, which leads to the 149.1 J energy regeneration. Therefore, although vibration isolation performance remains the same for these cases, part of the vibration energy is converted into electrical energy by HASAS.

Figure 14 shows the probability distribution of N for the three different objectives. It is shown that the situation $N = 0$ and $N = 2$ cannot be achieved for all of the three different control objectives. By combining the results in Table 1, the reasons for such phenomenon are visible. For that $N = 2$ cannot be realized, the main contradiction is between the soft damping state and stiff one. If the motor operates in regeneration mode under soft damping, it means that $|f_{refa}| < |f_{ed}|$ and $f_{refa} \cdot f_{ed} > 0$ (f_{refa} denotes the reference motor thrust under soft damping) in soft damping state. Then, if linear motor operates in energy consumption mode under medium state, it means that the oil damping force is too large and linear motor acts as a motor to provide an opposite thrust to offset part of oil damping force; that is, $f_{refb} \cdot f_{ed} < 0$ occurs (f_{refb} denotes the reference motor thrust in medium state). Therefore, when adjustable shock absorber is in stiff state, linear motor should still operate in consumption mode to offset part of oil damping force instead of regenerating energy. Vice versa, if linear motor operates in regeneration mode under stiff damping and consumption mode under medium damping, then it should still operate in consumption mode in soft state. With regard to $N = 0$, which means that the linear motor operates in regeneration mode under all the three damping levels, this problem may be solved by choosing the motor with larger back EMF coefficient, thrust coefficient, and lower internal resistance. In this way, the motor just operates as a generator that can produce the required active force without consuming electrical energy from the power source.

5.2. Bump Road Input. To evaluate the transient response characteristics of HASAS with respect to discrete irregularities, the road excitation is assumed as bump profile [28] and is described by

$$z_r = \begin{cases} \dfrac{A_m}{2}\left(1 - \cos\left(\dfrac{2\pi u}{L}t\right)\right), & 0 \le t \le \dfrac{L}{u}, \\ 0, & t \le \dfrac{L}{u}, \end{cases} \tag{28}$$

where A_m is the height of the bump profile and L is the bump width. Here A_m and L are set to be 0.08 m and 4 m, respectively. And the vehicle velocity u is set to be 10 m/s.

Figure 15 describes time responses of passive suspension and HASAS for the three control targets with bump road input. It can be seen that minimum sprung mass acceleration and tire dynamic load happen when ride comfort is stressed, followed by the values with trade-off control target. For handling, sprung mass acceleration and tire dynamic load are even larger than those of passive suspension. The time responses of HASAS for different control targets on bump road are different from those results on random road. The reason is that the frequency range of the bump input is mainly 0~5 Hz. The response characteristics of HASAS in relative low frequency regions under LQR control lead to the results. For sprung mass acceleration, minimum value for ride comfort (compared with trade-off, handling, and passive suspension) and maximum value for handling happen near all the frequency regions. As for tire dynamic load, ride comfort control target maintains minimum value from 0 Hz to 5 Hz and maximum value from 8 Hz to 12 Hz, while handling control target maintains opposite results (minimum value from 8 Hz to 15 Hz and maximum value from 2 Hz to 5 Hz).

The results of motor thrust of the 5 cases for three different control objectives are represented by Figure 16. Active suspension (Case A) demands high motor force for all of the three targets, especially for handling. Minimum peak values of motor thrust in HAPS (Cases B~D) happen in Cases D, C, and B for ride comfort, trade-off, and handling, respectively. It is worth noting that the motor peak thrust of Case B for ride comfort is even larger than that of active suspension,

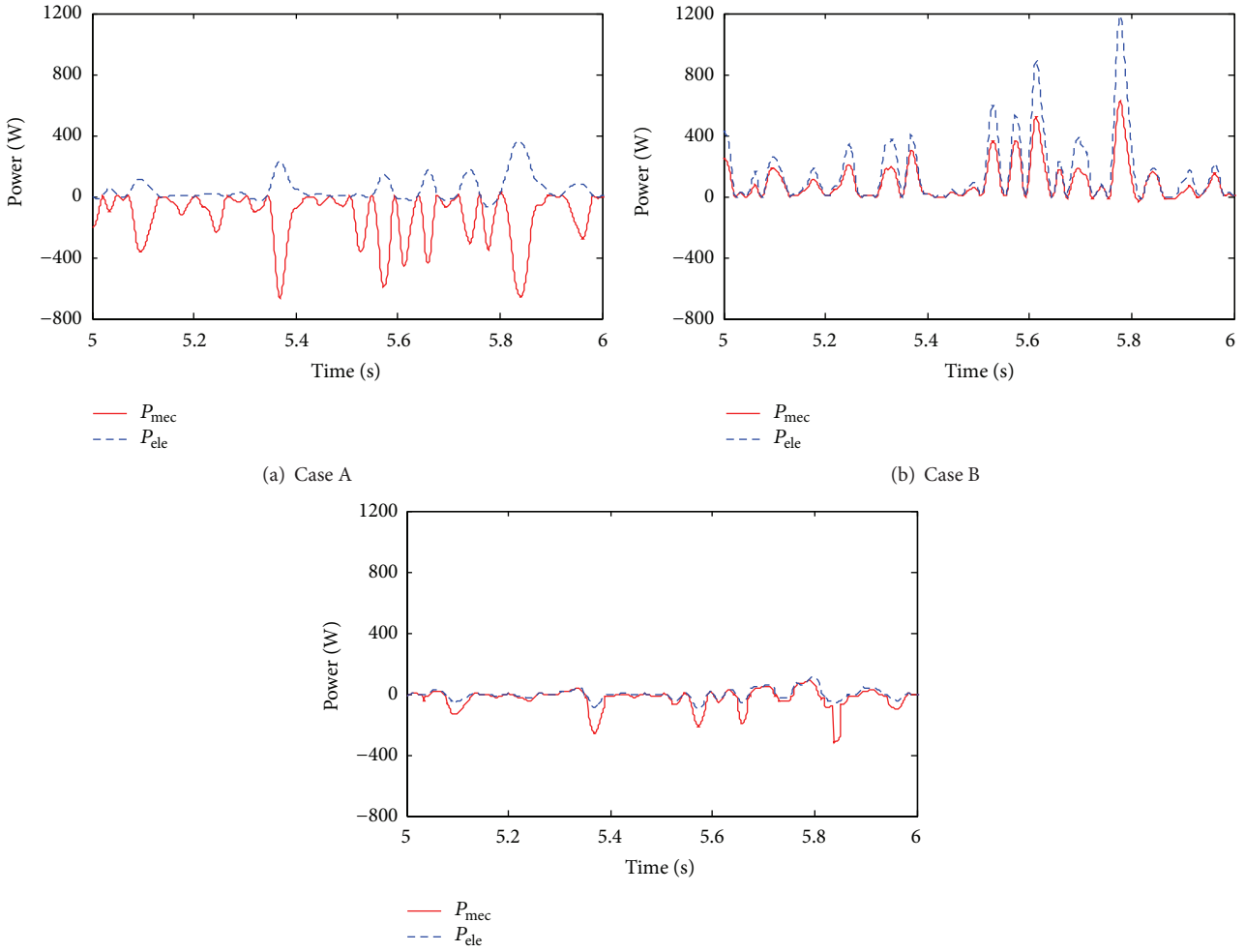

(a) Case A

(b) Case B

(c) Case E

Figure 13: Comparisons between P_{ele} and P_{mec}.

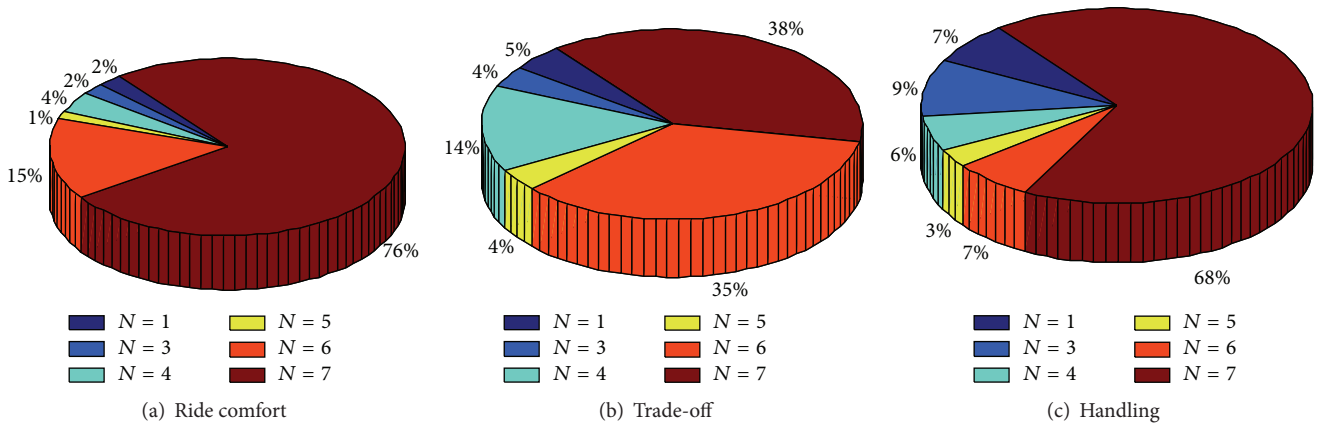

(a) Ride comfort

(b) Trade-off

(c) Handling

Figure 14: Probability of N for trade-off.

which means that large passive damping has a bad effect on reducing the motor action force when ride comfort is stressed. However, large passive damping shows a much smaller peak thrust when handling is emphasized. From Figure 16, it is also apparent that motor thrust of HASAS (Case E) follows along the thrust trajectories of Cases B, C, and D in different time regions. Such phenomenon denotes that HASAS switches among different damping values to ensure the superior performance in reducing motor thrust for different control targets.

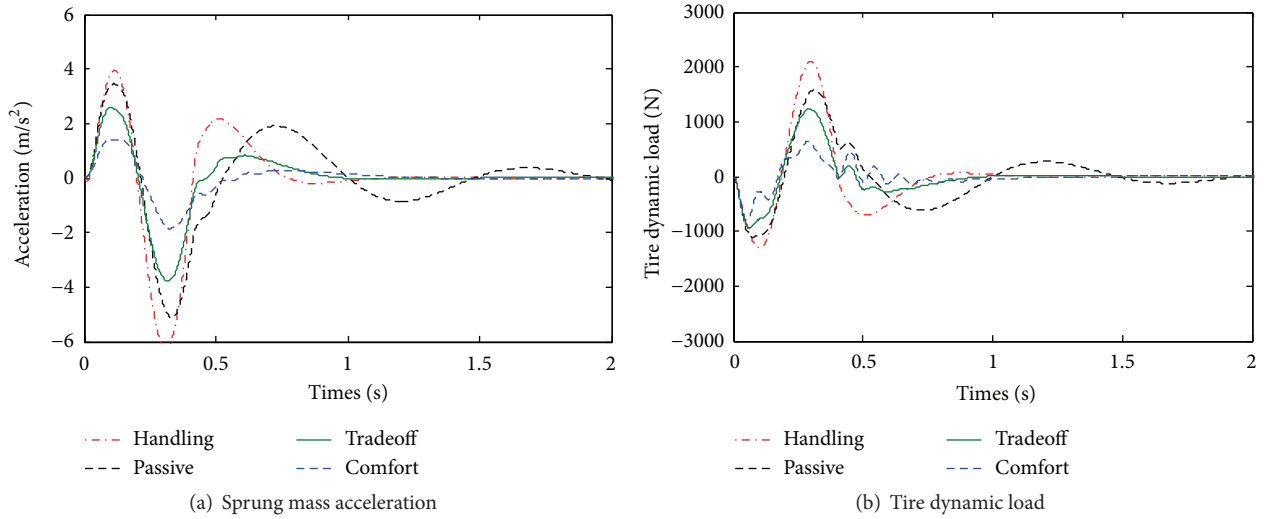

(a) Sprung mass acceleration (b) Tire dynamic load

FIGURE 15: Actual responses of the proposed suspension comparing to passive suspension.

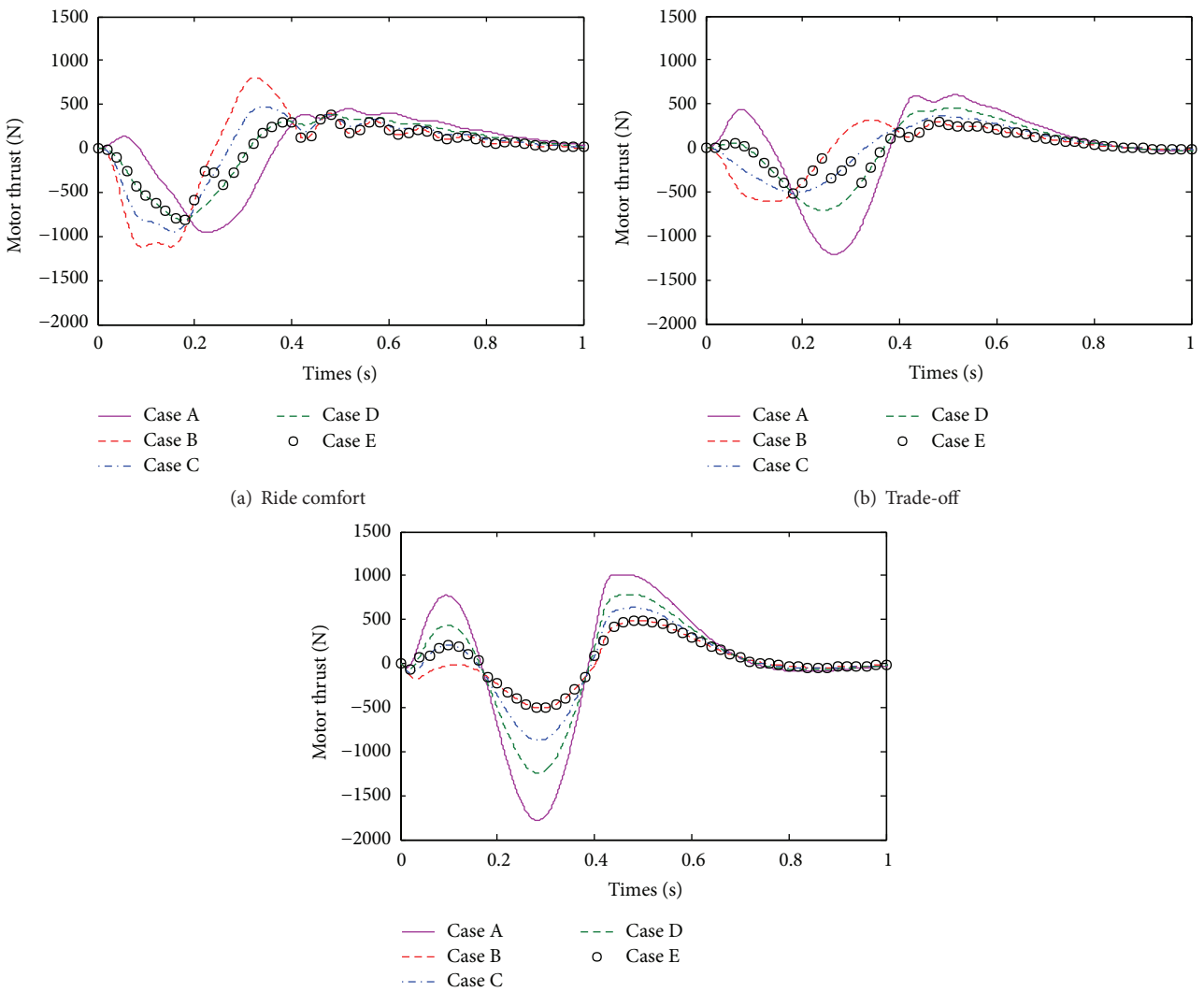

(a) Ride comfort (b) Trade-off

(c) Handling

FIGURE 16: Motor thrust with different control targets.

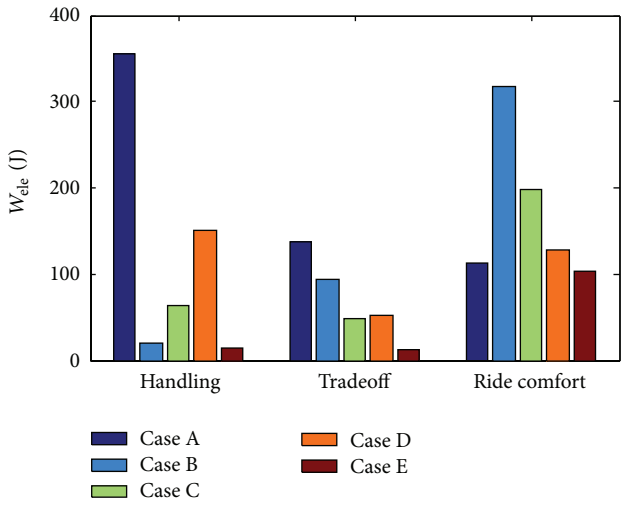

Figure 17: Energy consumption of linear motor with bump road.

With respect to the discrete bump input, energy consumption of linear motor from Cases A~E for the three control targets is shown in Figure 17. It shows that less energy consumption with small damping (Case D) and more energy consumption with large damping (Case B) for ride comfort happen. For handling, large damping is a better choice to reduce energy consumption, while small damping corresponds to large energy consumption. Meanwhile, energy consumption of HASAS is least for all of the three control objectives with bump input. The superiority of HASAS in energy conservation is validated.

6. Conclusions

This paper proposes the concept of HASAS by integrating the adjustable shock absorber with a linear motor. By providing three kinds of base damping force, the adjustable shock absorber can not only reduce demands on the linear motor rated capacity, but also tune the motor operating points to realize energy conservation for various control targets and even ensure energy regeneration. Based on the energy flow principle between linear motor and the power source, the mode decision and switch controller is developed. And the system controller is further designed to exert the superiority of HASAS.

Simulation results validate the effectiveness of the proposed suspension system under random road and bump road inputs. Compared to active suspension and HAPS, the motor peak and RMS thrust are reduced apparently while the same vibration isolation performance can be achieved. Although energy conservation of HASAS for ride comfort objective cannot be achieved compared to the active suspension with random road excitation, HASAS is superior for handing and trade-off objectives. Energy conservation of HASAS is suitable for various control objectives. Study on the impact of adjustable damping on motor power consumption is helpful for the optimization of motor operation points to improve energy regeneration performance. By harmonizing the adjustable shock absorber and linear motor, self-powered active control is realized, and even extra regenerative energy stored into the power source can also be obtained. Moreover, the energy conservation performance can be further improved by expanding the range of adjustable damping.

In our further study, the real linear motor will be integrated into the trial produced adjustable shock absorber. The real controller especially the thrust controller will be developed to realize the motor active control on practical bench test to testify HASAS and analyze energy consumption of linear motor. In fact, since EV and HEV have their own electrical power source, the usage of energy regenerative suspension in new energy vehicles to coordinate the suspension dynamic performance (ride comfort, handling) and energy consumption performance of power source (energy consumption and regeneration) is of great significance.

Conflict of Interests

The authors declare that there is no conflict of interests regarding the publication of this paper.

Acknowledgments

The authors would like to express their great gratitude for the support from the project funded by the Priority Academic Program Development of Jiangsu Higher Education Institutions (PAPD), the National Natural Science Foundation of China (Grant no. 51407086), the Natural Science Foundation of Jiangsu Province (BK 2012714), Project funded by China Postdoctoral Science Foundation (2014M551518), and the Scientific Research Innovation Projects of Jiangsu Province (KYLX_1022). The authors would also like to thank the editors for improving the readability of the paper.

References

[1] B. L. J. Gysen, J. L. G. Janssen, J. J. H. Paulides, and E. A. Lomonova, "Design aspects of an active electromagnetic suspension system for automotive applications," *IEEE Transactions on Industry Applications*, vol. 45, no. 5, pp. 1589–1597, 2009.

[2] S. Lee and W.-J. Kim, "Active suspension control with direct-drive tubular linear brushless permanent-magnet motor," *IEEE Transactions on Control Systems Technology*, vol. 18, no. 4, pp. 859–870, 2010.

[3] B. L. J. Gysen, J. J. H. Paulides, J. L. G. Janssen, and E. A. Lomonova, "Active electromagnetic suspension system for improved vehicle dynamics," *IEEE Transactions on Vehicular Technology*, vol. 59, no. 3, pp. 1156–1163, 2010.

[4] I. Martins, J. Esteves, G. D. Marques, and F. P. da Silva, "Permanent-magnets linear actuators applicability in automobile active suspensions," *IEEE Transactions on Vehicular Technology*, vol. 55, no. 1, pp. 86–94, 2006.

[5] Y. Suda and T. Shiiba, "A new hybrid suspension system with active control and energy regeneration," *Vehicle System Dynamics*, vol. 25, supplement 1, pp. 641–654, 1996.

[6] K. Nakano, "Combined type self-powered active vibration control of truck cabins," *Vehicle System Dynamics*, vol. 41, no. 6, pp. 449–473, 2004.

[7] W. Hu and N. M. Wereley, "Hybrid magnetorheological fluid-elastomeric lag dampers for helicopter stability augmentation," *Smart Materials and Structures*, vol. 17, no. 4, Article ID 045021, 2008.

[8] Y. Suda, S. Nakadai, and K. Nakano, "Hybrid suspension system with skyhook control and energy regeneration (development of self-powered active suspension)," *Vehicle System Dynamics*, vol. 29, supplement 1, pp. 619–634, 1998.

[9] K. Nakanoa, Y. Suda, and S. Nakadai, "Self-powered active vibration control using a single electric actuator," *Journal of Sound and Vibration*, vol. 260, no. 2, pp. 213–235, 2003.

[10] G. Zhang, J. Cao, and F. Yu, "Design of active and energy-regenerative controllers for DC-motor-based suspension," *Mechatronics*, vol. 22, no. 8, pp. 1124–1134, 2012.

[11] L. Zuo, B. Scully, J. Shestani, and Y. Zhou, "Design and characterization of an electromagnetic energy harvester for vehicle suspensions," *Smart Materials and Structures*, vol. 19, no. 4, Article ID 045003, 2010.

[12] Z. Li, L. Zuo, G. Luhrs, L. Lin, and Y.-X. Qin, "Electromagnetic energy-harvesting shock absorbers: design, modeling, and road tests," *IEEE Transactions on Vehicular Technology*, vol. 62, no. 3, pp. 1065–1074, 2013.

[13] Z. Li, L. Zuo, J. Kuang, and G. Luhrs, "Energy-harvesting shock absorber with a mechanical motion rectifier," *Smart Materials and Structures*, vol. 22, no. 2, Article ID 025008, 2013.

[14] Y. Akami, H. Chikuma, S. Ohsawa et al., "Electromagnetic suspension system," US Patent 7,219,781, 2007.

[15] B. Ebrahimi, M. B. Khamesee, and F. Golnaraghi, "Design of a hybrid electromagnetic/hydraulic damper for automotive suspension systems," in *Proceedings of the IEEE International Conference on Mechatronics and Automation (ICMA '09)*, pp. 3196–3200, Changchun, China, August 2009.

[16] B. Ebrahimi, H. Bolandhemmat, M. B. Khamesee, and F. Golnaraghi, "A hybrid electromagnetic shock absorber for active vehicle suspension systems," *Vehicle System Dynamics*, vol. 49, no. 1-2, pp. 311–332, 2011.

[17] I. Martins, J. Esteves, F. Pina da Silva, and P. Verdelho, "Electromagnetic hybrid active-passive vehicle suspension system," in *Proceedings of the IEEE 49th Vehicular Technology Conference*, vol. 3, pp. 2273–2277, Houston, Tex, USA, July 1999.

[18] B. L. J. Gysen, T. P. J. van der Sande, J. J. H. Paulides, and E. A. Lomonova, "Efficiency of a regenerative direct-drive electromagnetic active suspension," *IEEE Transactions on Vehicular Technology*, vol. 60, no. 4, pp. 1384–1393, 2011.

[19] Q.-H. Nguyen and S.-B. Choi, "Optimal design of MR shock absorber and application to vehicle suspension," *Smart Materials and Structures*, vol. 18, no. 3, Article ID 035012, 2009.

[20] H. Chen, C. Long, C.-C. Yuan, and H.-B. Jiang, "Non-linear modelling and control of semi-active suspensions with variable damping," *Vehicle System Dynamics*, vol. 51, no. 10, pp. 1568–1587, 2013.

[21] H.-B. Jiang, Y.-J. Du, and S.-C. Ye, "Stroke-dependent stiffness characteristics of a new type of integrated suspension strut," *Journal of Vibration and Shock*, vol. 31, no. 22, pp. 66–70, 2012.

[22] X.-M. Dong, M. Yu, C.-R. Liao, and W.-M. Chen, "Comparative research on semi-active control strategies for magneto-rheological suspension," *Nonlinear Dynamics*, vol. 59, no. 3, pp. 433–453, 2010.

[23] R. C. Wang, H. B. Jiang, L. Chen et al., "Modelling and control of semi-active susppension with nonlinear damping," *Transactions of the Chinese Society for Agricultural Machinery*, vol. 39, no. 12, pp. 14–17, 2008.

[24] Y. Kawamoto, Y. Suda, H. Inoue, and T. Kondo, "Modeling of electromagnetic damper for automobile suspension," *Journal of System Design and Dynamics*, vol. 1, no. 3, pp. 524–535, 2007.

[25] K. Huang, Y.-C. Zhang, F. Yu, and Y.-H. Gu, "Coordinate optimization for synthetical performance of electrical energy-regenerative active suspension," *Journal of Shanghai Jiaotong University*, vol. 43, no. 2, pp. 226–230, 2009.

[26] H. Kim, J. Son, and J. Lee, "A high-speed sliding-mode observer for the sensorless speed control of a PMSM," *IEEE Transactions on Industrial Electronics*, vol. 58, no. 9, pp. 4069–4077, 2011.

[27] Y. He and F. L. Luo, "Sliding-mode control for dc-dc converters with constant switching frequency," *IEE Proceedings: Control Theory and Applications*, vol. 153, no. 1, pp. 37–45, 2006.

[28] H. Li, J. Yu, C. Hilton, and H. Liu, "Adaptive sliding-mode control for nonlinear active suspension vehicle systems using T-S fuzzy approach," *IEEE Transactions on Industrial Electronics*, vol. 60, no. 8, pp. 3328–3338, 2013.